Electronic Research Archive

ERA, 30(9): 3249–3265.
DOI: 10.3934/era.2022165
Received: 06 May 2022
Revised: 08 June 2022
Accepted: 14 June 2022
Published: 21 June 2022

http://www.aimspress.com/journal/ERA

Research article

Joint linear array structure and waveform design for MIMO radar under practical constraints

Chunhua Chu[1,2], Yijun Chen[3,*], Qun Zhang[1] and Ying Luo[1]

[1] Information and Navigation College, Air Force Engineering University, Xi'an, Shaanxi 710077, China
[2] Mechanical and Electrical Engineering College, Hainan University, Haikou, Hainan 570228, China
[3] College of Information Engineering, Engineering University of PAP, Xi'an, Shaanxi 710078, China

* **Correspondence:** Email: chenyijun519@126.com; Tel: +8615399487213.

Abstract: Optimizing the array structure or emission waveform of a multiple-input multiple-output (MIMO) radar system is an effective method to improve the performance in practical applications. In this study, the joint optimization of array structure and the corresponding emission waveform under interference and noise conditions was investigated. When compared with the waveform or array structure optimization alone, this method allowed the MIMO radar system to obtain a higher degree of freedom. By considering the practical limitations of the MIMO radar system, a waveform with good properties, such as orthogonality or pulse compression performance, was selected as the reference waveform. Subsequently, based on the similarity constraint and constant modulus constraint, a bivariate joint optimization problem of array structure and waveform was formulated, and an iterative optimization algorithm was proposed to solve it. The array composition was determined using a combinatorial search algorithm while the emission waveform was obtained by solving the similarity model. Eventually, it effectively converged to form quasi-optimal match variables after limited iterations. The proposed method can be expanded to the optimal launch of a specific target and an environment with a proper or minimum number of antennas, as well as implement array optimization with the desired waveform. The simulation results prove the effectiveness of the proposed method. This method provides an ideal choice for real-time construction, flexible launch, and signal processing of MIMO radar systems.

Keywords: waveform optimization; array structure design; signal-to-interference-noise ratio (SINR); fractional programming; generalized power-like iteration method (GPLIM)

1. Introduction

The MIMO radar was developed as a result of the multiple-input multiple-output (MIMO) technology in communication systems [1,2]. The main difference between MIMO radar and the phased array radar is that each antenna of MIMO radar can independently transmit arbitrary waveforms, and the receiving end can perform diversity processing on the signal [3,4]. Under the condition of the same number of antennas, the diversity of waveforms allows the MIMO radar to outperform the phased array radar in terms of target detection [5,6], such as higher spatial resolution [7,8] and DOA estimation [9]. Therefore, the waveform design problem for the MIMO radar is a hot spot. Based on different design goals, the MIMO radar waveform optimization is divided into the following categories. The first type is to design the emission waveform to achieve the desired pattern when the target or interference airspace direction is prior information [10−12]; the second type is the orthogonal emission waveform design for achieving signal diversity at the receiving end [13,14]; the third category is to design waveform based on the joint signal processing of the radar transceiver system for different goals, such as maximizing the output signal-to-interference-noise ratio (SINR) [15,16] or maximizing the mutual information (MI) of target response and the echo [17,18]. In addition, real-time agile cognitive waveform design through environmental perception and echo feedback to the transmitter can be achieved [19,20].

All of the above studies are based on the consideration of fixed arrays. Here, we consider the joint design of transmit waveform and array structure, which supplies additional degrees of freedom at the transmitter. In [21] and [22], an efficient method of waveform covariance matrix design and antenna selection was developed. However, few works have been devoted to the joint design of array structure and waveform based on the consideration of signal reliability or quality at the receiver under interference and noise conditions, which is more challenging and practical for MIMO radar systems. This study aims to obtain a high-quality signal at the receiver of the MIMO radar by joint optimization of array structure and emission waveform with the practical constraint of constant modulus and similarity constraint (SC) in a signal-dependent interference environment. The main task of this study is to successfully optimize the joint objective of maximizing the SINR and proper array structure under a specific number of transmit and receive array elements with the constant modulus constraint (CMC) and SC. Specifically, to solve the resulted non-convex joint optimization problem, an efficient alternate iterative optimization algorithm based on fractional programming and generalized power-like iteration (GPLIM) is developed such that the SINR is improved while the responding radar array structure is obtained. The numerical results demonstrate the effectiveness and efficiency of the proposed algorithm.

The remainder of this paper is organized as follows. The signal and array structure models are introduced in Section 2. In Section 3, the practical constraints of emission waveform and partial-array structure design problems are discussed, and a joint optimization model is established. Based on fractional programming and GPLIM, an iterative optimization algorithm for the joint design is developed in Section 4. Section 5 presents various numerical simulations and analyses of the experimental results. Finally, the conclusions are drawn in Section 6.

Notation: We use $\boldsymbol{a}$ (lowercase, boldface) or A (uppercase, italics) for vector, and $\mathbf{A}$ (uppercase, boldface) for matrix. $(\cdot)^T$, $(\cdot)^*$, and $(\cdot)^H$ denote the transpose, conjugate, and conjugate transpose, respectively. $\mathrm{vec}(\mathbf{A})$ denotes a column vector obtained by stacking the columns of $\mathbf{A}$ on top of one another. $\mathbf{A}\succ 0$ indicates that the matrix $\mathbf{A}$ is positive definite. $\mathbf{I}_N$ represents the $N\times N$ identity matrix. Finally, we use $\odot$ and $\otimes$ to denote the Hadamard product and Kronecker product, respectively. $E(\cdot)$ represents the expectation of a random variable; $\arg(x)$ represents the angle of x.

2. MIMO radar signal model and array structure

This study mainly deals with the fast-time radar waveform design; therefore, the Doppler frequency of the target is ignored. In addition, information regarding interference and target, such as the direction and the radar cross section can be acquired from a professional database or obtained through the cognitive working mode of the radar. Based on these instructions, a centralized MIMO radar system equipped with M antennas is considered, assuming the array is a uniform linear array with half-a-wavelength element separation. Suppose that the total emission energy of the radar system is $E = N_t * K$. As shown in Figure 1, the numbers of effective emission and receiving antennas of the optimized partial-array are N_t and N_r, where $N_t \le N_r \le M$.

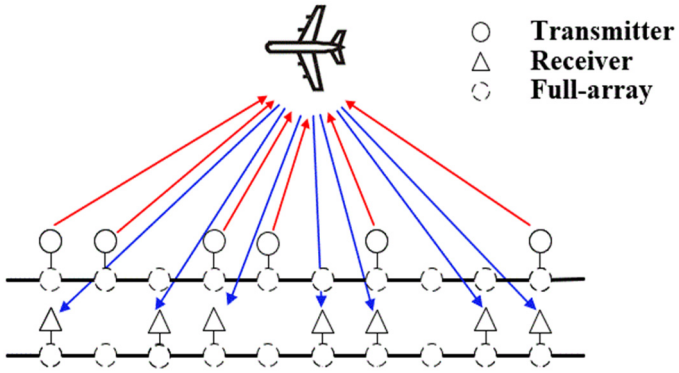

Figure 1. Schematic diagram of MIMO radar array structure.

The effective vector of array elements can be expressed as

$$P=[p_1,...,p_m,...,p_M]^T. \tag{1}$$

when p_m is 1, it means that the mth antenna of the array element position is valid; when p_m is 0, it means that the mth antenna of the array element position does not work. Further, P_t and P_r denote the effective vectors of transmit and receive array, respectively.

$$P_t=[p_{1t},...,p_{mt},...,p_{Mt}]^T, P_r=[p_{1r},...,p_{mr},...,p_{Mr}]^T. \tag{2}$$

Suppose s_m is the sampling sequence of the transmitted signal of the mth array element, and K represents the sequence length. The emission signal of MIMO radar can be expressed as

$$\mathbf{S}=[\boldsymbol{s}_1,\boldsymbol{s}_2,...,\boldsymbol{s}_M]^T=[\boldsymbol{s}(1),...,\boldsymbol{s}(k),...,\boldsymbol{s}(K)]=\begin{bmatrix} \boldsymbol{s}_1(1) & \boldsymbol{s}_1(2) & ... & \boldsymbol{s}_1(K) \\ \boldsymbol{s}_2(1) & \boldsymbol{s}_2(2) & ... & \boldsymbol{s}_2(K) \\ ... & ... & ... & ... \\ \boldsymbol{s}_M(1) & \boldsymbol{s}_M(2) & ... & \boldsymbol{s}_M(K) \end{bmatrix} \tag{3}$$

where $\boldsymbol{s}_m=[s_m(1),s_m(2),...,s_m(K)]^T$, and $\boldsymbol{s}(k)=[s_1(k),...,s_2(k),...,s_M(k)]^T$ denotes the sequence at the k th sampling time of the full-array. Considering array structure optimization, the actual transmit waveform can be expressed as

$$\mathbf{S}^*=[\boldsymbol{s}_1,\boldsymbol{s}_2,...,\boldsymbol{s}_M]^T\odot P_t=[\boldsymbol{s}_1\otimes p_{1t},\boldsymbol{s}_2\otimes p_{2t},...,\boldsymbol{s}_M\otimes p_{Mt}]^T. \tag{4}$$

To facilitate the calculation, an array element position optimization matrix $P_t^*=P_t \cdot ones(1,K)$ is introduced, and Eq (4) can be recast as

$$\mathbf{S}^* = \mathbf{S} \odot P_t^* = \begin{bmatrix} \boldsymbol{s}_1(1)\cdot p_{1t} & \boldsymbol{s}_1(2)\cdot p_{1t} & \ldots & \boldsymbol{s}_1(K)\cdot p_{1t} \\ \boldsymbol{s}_2(1)\cdot p_{2t} & \boldsymbol{s}_2(2)\cdot p_{2t} & \ldots & \boldsymbol{s}_2(K)\cdot p_{2t} \\ \ldots & \ldots & \ldots & \ldots \\ \boldsymbol{s}_M(1)\cdot p_{Mt} & \boldsymbol{s}_M(2)\cdot p_{Mt} & \ldots & \boldsymbol{s}_M(K)\cdot p_{Mt} \end{bmatrix}. \tag{5}$$

Assuming that the target direction θ_t is a priori, the reflected signal of the target in this direction received by MIMO radar is

$$\mathbf{Y}_t = \alpha_t \boldsymbol{a}_{rp}(\theta_t)\boldsymbol{a}_{tp}{}^T(\theta_t)\mathbf{S}^* \tag{6}$$

where α_t denotes the complex amplitudes of target; $\boldsymbol{a}_{tp}(\theta_t)$ and $\boldsymbol{a}_{rp}(\theta_t)$ are the steering vectors of the radar transmit and receive arrays, respectively. Further, $\boldsymbol{a}_{tp}(\theta_t)$ and $\boldsymbol{a}_{rp}(\theta_t)$ can be expressed as

$$\begin{aligned} \boldsymbol{a}_{tp}(\theta_t) &= \boldsymbol{a}_t(\theta_t)\odot P_t = \left[1, e^{-j\pi\sin(\theta_t)}, \ldots, e^{-j\pi(M-1)\sin(\theta_t)}\right]^T \odot P_t, \\ \boldsymbol{a}_{rp}(\theta_t) &= \boldsymbol{a}_r(\theta_t)\odot P_r = \left[1, e^{-j\pi\sin(\theta_t)}, \ldots, e^{-j\pi(M-1)\sin(\theta_t)}\right]^T \odot P_r. \end{aligned} \tag{7}$$

When the transmit and receive array vectors are equal, $\boldsymbol{a}_{rp}(\theta_t)=\boldsymbol{a}_{tp}(\theta_t)$.

By taking the target location as the reference point, the direction of the nth signal-dependent interference is θ_n, $n=1,\ldots,N_c$, $\theta_n \neq \theta_t$. The clutter signal at the receive array is given by

$$\mathbf{Y}_c = \sum_{n=1}^{N_c} \alpha_n \boldsymbol{a}_{rp}(\theta_n)\boldsymbol{a}_{tp}{}^T(\theta_n)\mathbf{S}^* \tag{8}$$

where α_n denotes the complex amplitude of the nth signal-dependent interference. Let $\mathbf{N} \in C^{M\times K}$ be the received white Gaussian noise, and the variance be σ^2. Because both the steering vector $\boldsymbol{a}_{tp}(\theta_t)$ and emission signal $\mathbf{S}^*$ are multiplied by P_t, the baseband equivalent of signals at the receive array can be described as

$$\begin{aligned} \mathbf{Y} &= \mathbf{Y}_t + \mathbf{Y}_c + \mathbf{N} = \alpha_t \boldsymbol{a}_{rp}(\theta_t)\boldsymbol{a}_{tp}{}^T(\theta_t)\mathbf{S}^* + \sum_{n=1}^{N_c}\alpha_n \boldsymbol{a}_{rp}(\theta_n)\boldsymbol{a}_{tp}{}^T(\theta_n)\mathbf{S}^* + \mathbf{N} \\ &= \alpha_t \boldsymbol{a}_{rp}(\theta_t)\boldsymbol{a}_{tp}{}^T(\theta_t)\mathbf{S} + \sum_{n=1}^{N_c}\alpha_n \boldsymbol{a}_{rp}(\theta_n)\boldsymbol{a}_{tp}{}^T(\theta_n)\mathbf{S} + \mathbf{N}. \end{aligned} \tag{9}$$

By stacking all the columns of $\mathbf{Y}$ into a vector, Eq (9) can be recast as

$$\boldsymbol{y} = \boldsymbol{y}_t + \boldsymbol{y}_c + \boldsymbol{n} = \alpha_t \mathbf{A}(\theta_t)\boldsymbol{x} + \sum_{n=1}^{N_c}\alpha_n \mathbf{A}(\theta_n)\boldsymbol{x} + \boldsymbol{n} \tag{10}$$

where $\boldsymbol{y}=\mathrm{vec}(\mathbf{Y})$; $\boldsymbol{x}=\mathrm{vec}(\mathbf{S})=[\boldsymbol{s}^T(1),\boldsymbol{s}^T(2),\ldots,\boldsymbol{s}^T(K)]^T$; $\boldsymbol{n}=\mathrm{vec}(\mathbf{N})\in C^{KN_r*1}$ is a circular complex Gaussian noise vector with zero mean and covariance matrix $\sigma_n^2\mathbf{I}_{N_r,K}$; $\mathbf{A}(\theta_t)=\mathbf{I}_K \otimes (\boldsymbol{a}_{rp}(\theta_t)\boldsymbol{a}_{tp}{}^T(\theta_t))$ and $\mathbf{A}(\theta_n)=\mathbf{I}_K \otimes (\boldsymbol{a}_{rp}(\theta_n)\boldsymbol{a}_{tp}{}^T(\theta_n))$ denote the transceiver joint steering matrix of the MIMO radar in target and jammer directions, respectively.

3. Practical constraints and problem formulation

Because the target detection performance is determined by the output SINR of the MIMO radar system, this section takes the SINR maximization as the optimization goal to design the array structure and emission waveform simultaneously for the MIMO radar in the presence of signal dependent interferences. From (10), the output SINR can be modeled as

$$\mathrm{SINR}=\frac{E\left\{\alpha_t \boldsymbol{x}^H \mathbf{A}^H(\theta_t)\alpha_t \mathbf{A}(\theta_t)\boldsymbol{x}\right\}}{\sum_{n=1}^{N_c} E\left\{\alpha_n \boldsymbol{x}^H \mathbf{A}^H(\theta_n)\alpha_n \mathbf{A}(\theta_n)\boldsymbol{x}\right\}+E(\boldsymbol{n}^H\boldsymbol{n})}=\frac{\frac{\left(|\alpha_t|^2\right)}{\sigma_n^2}\cdot\left\{\boldsymbol{x}^H \mathbf{A}^H(\theta_t)\mathbf{A}(\theta_t)\boldsymbol{x}\right\}}{\boldsymbol{x}^H\left\{\sum_{n=1}^{N_c}\frac{\left(|\alpha_n|^2\right)}{\sigma_n^2}\mathbf{A}^H(\theta_n)\mathbf{A}(\theta_n)\right\}\boldsymbol{x}+KN_r}. \tag{11a}$$

Denote $\mathrm{SNR}=E\left(|\alpha_t|^2\right)/\sigma_n^2$; $\mathrm{INR}_n=E\left(|\alpha_n|^2\right)/\sigma_n^2$, $\boldsymbol{\Sigma}(\theta_n)=\sum_{n=1}^{N_c}\mathrm{INR}_n\mathbf{A}^H(\theta_n)\mathbf{A}(\theta_n)$, $n=1,...,N_c$; $E(\boldsymbol{n}^H\boldsymbol{n})=KN_r\sigma_n^2$; $\forall\theta$, $\mathbf{A}(\theta)=\mathbf{I}_K\otimes(\mathbf{P}\odot(\boldsymbol{a}_r(\theta)\boldsymbol{a}_t^T(\theta)))=\mathbf{I}_K\otimes(\mathbf{P}\odot\mathbf{D}(\theta))$, $\mathbf{D}(\theta)=\boldsymbol{a}_r(\theta)\boldsymbol{a}_t^T(\theta)$; $\mathbf{P}=P_rP_t^T$. Simplifying the above formula, we obtain

$$\begin{aligned}\mathrm{SINR}&=\frac{\frac{\left(|\alpha_t|^2\right)}{\sigma_n^2}\cdot\left\{\boldsymbol{x}^H \mathbf{A}^H(\theta_t)\mathbf{A}(\theta_t)\boldsymbol{x}\right\}}{\boldsymbol{x}^H\left\{\sum_{n=1}^{N_c}\frac{\left(|\alpha_n|^2\right)}{\sigma_n^2}\mathbf{A}^H(\theta_n)\mathbf{A}(\theta_n)\right\}\boldsymbol{x}+KN_r}\\&=\frac{\boldsymbol{x}^H\left\{\mathrm{SNR}\cdot(\mathbf{I}_K\otimes(\mathbf{P}\odot\mathbf{D}(\theta_t)))^H(\mathbf{I}_K\otimes(\mathbf{P}\odot\mathbf{D}(\theta_t)))\right\}\boldsymbol{x}}{\boldsymbol{x}^H\left\{\sum_{n=1}^{N_c}\mathrm{INR}_n\cdot\left\{(\mathbf{I}_K\otimes(\mathbf{P}\odot\mathbf{D}(\theta_n)))^H(\mathbf{I}_K\otimes(\mathbf{P}\odot\mathbf{D}(\theta_n)))\right\}\right\}\boldsymbol{x}+KN_r}\end{aligned}. \tag{11b}$$

The output SINR of the MIMO radar system is determined by the radar transmit waveform and the joint structure matrix of the transmit and receive array under the condition that the target and clutter direction, scattering power, and other information are known a priori. The structure matrix $\mathbf{P}$ of the array and the transmit waveform vector $\boldsymbol{x}$ can effectively improve the quality of the radar output signal.

Considering the nonlinear limitation of the power amplifier in the radar system, it is reasonable to enforce a peak-to-average ratio (PAR) constraint on each antenna, that is,

$$\mathrm{PAR}(\boldsymbol{s}_m)=\frac{\max_k|s_m(k)|^2}{\frac{1}{K}\sum_{k=1}^{K}|s_m(k)|^2}\le\rho,\quad \rho\in[1,K],\quad m=1,...,M. \tag{12}$$

When $\rho=1$, constant modulus codes can be obtained, and a modulus value of 1 can be calculated according to the emission energy. The CMC is the strictest PAR constraint. In addition, to ensure some characteristics of emission waveform, a SC should also be imposed on the waveform, that is,

$$\|\boldsymbol{x}-\boldsymbol{x}_0\|^2\le\varepsilon \tag{13}$$

where $\boldsymbol{x}_0$ is a reference waveform with desired properties, and parameter $0 \le \varepsilon \le 2$ rules the extent of the similarity [23,24]. By considering the constant modulus constraint, the similarity constraint (13) can be further recast as

$$\arg x(i) \in [\gamma_i - \alpha, \gamma_i + \alpha], \quad i = 1,...,MK \tag{14}$$

where $\gamma_i = \arg \boldsymbol{x}_0(i), i = 1,...,MK$, and $\alpha = \arccos(1-\varepsilon^2/2)$.

To maximize the SINR under the CMC and SC [23], the following problem should to be addressed:

$$\begin{aligned} &\max_{\mathbf{P},\boldsymbol{x}} \text{SINR} \\ &s.t.\ \arg x(i) \in [\gamma_i - \alpha, \gamma_i + \alpha] \\ &\quad |x(i)| = 1 \quad i = 1,...,MK. \end{aligned} \tag{15}$$

Equation (15) expresses a multivariate joint optimization problem. Compared with the existing approaches, the feasible set of waveforms is broadened owing to the simultaneous optimization of the transmit and receive arrays.

4. Optimization algorithm for the joint design of transmit waveform and array structure

The optimization problem in Eq (15) is non-convex and has no closed-form solution; thus, in the following section a sequential optimization algorithm is introduced to address this NP-hard problem. Specifically, this study iteratively optimizes one variable of $(\boldsymbol{x}, \mathbf{P})$ with the other variable fixed by maximizing the objective of Eq (11). Meanwhile, the values of P_t and P_r are updated with the achieved SINR at each iteration.

4.1. Optimizing $\mathbf{P}$ *with fixed* $\boldsymbol{x}$

According to Eq (11), the CMC and SC have no relationship with $\mathbf{P}$. Hence, with fixed $\boldsymbol{x}$, optimization problem in Eq (15) with respect to $\mathbf{P}$ can be recast as

$$\max_{\mathbf{P}} \frac{\boldsymbol{x}^H \left\{ \text{SNR} \cdot (\mathbf{I}_K \otimes (\mathbf{P} \odot \mathbf{D}(\theta_t)))^H (\mathbf{I}_K \otimes (\mathbf{P} \odot \mathbf{D}(\theta_t))) \right\} \boldsymbol{x}}{\boldsymbol{x}^H \left\{ \sum_{n=1}^{N_c} \text{INR}_n \cdot \left\{ (\mathbf{I}_K \otimes (\mathbf{P} \odot \mathbf{D}(\theta_n)))^H (\mathbf{I}_K \otimes (\mathbf{P} \odot \mathbf{D}(\theta_n))) \right\} \right\} \boldsymbol{x} + KN_r}. \tag{16}$$

As the array structure matrix $\mathbf{P}$ is a matrix of 0-1 elements, $\mathbf{P} = P_r P_t^T$. P_t and P_r can be generated through enumeration, and then $\mathbf{P}$ can be synthesized.

4.2. Optimizing $\boldsymbol{x}$ *with fixed* $\mathbf{P}$

With a fixed $\mathbf{P}$, Eq (15) with respect to $\boldsymbol{x}$ can be equivalent to

$$\begin{aligned} &\max_{\boldsymbol{x}} \frac{\boldsymbol{x}^H \left\{ \text{SNR} \cdot (\mathbf{I}_K \otimes (\mathbf{P} \odot \mathbf{D}(\theta_t)))^H (\mathbf{I}_K \otimes (\mathbf{P} \odot \mathbf{D}(\theta_t))) \right\} \boldsymbol{x}}{\boldsymbol{x}^H \left\{ \sum_{n=1}^{N_c} \text{INR}_n \cdot \left\{ (\mathbf{I}_K \otimes (\mathbf{P} \odot \mathbf{D}(\theta_n)))^H (\mathbf{I}_K \otimes (\mathbf{P} \odot \mathbf{D}(\theta_n))) \right\} \right\} \boldsymbol{x} + KN_r}, \\ &s.t.\ \arg x(i) \in [\gamma_i - \alpha, \gamma_i + \alpha], \\ &\quad |x(i)| = 1 \quad i = 1,...,MK. \end{aligned} \tag{17}$$

As the power emitted by an antenna is $\sum_{k=1}^{K}\boldsymbol{s}^H(k)\boldsymbol{s}(k)=K$, the amplitude of the kth code is 1. Using fractional programming as in [25], the above problem can be approximately equivalent to

$$\begin{aligned}&\max_{\boldsymbol{x}}\ \boldsymbol{x}^H\left(\mathbf{U}(\theta_t)\text{-}\lambda^{(r)}\left[\boldsymbol{\Sigma}(\theta_n)+\frac{N_r}{M}\mathbf{I}_{MK}\right]\right)\boldsymbol{x},\\&s.t.\ \arg x(i)\in[\gamma_i-\alpha,\gamma_i+\alpha],\\&\quad |x(i)|=1\quad i=1,...,MK.\end{aligned}\tag{18}$$

where $\mathbf{U}(\theta_t)=\mathrm{SNR}\cdot(\mathbf{I}_K\otimes(\mathbf{P}\odot\mathbf{D}(\theta_t)))^H(\mathbf{I}_K\otimes(\mathbf{P}\odot\mathbf{D}(\theta_t)))$, $\boldsymbol{\Sigma}(\theta_n)=\sum_{n=1}^{N_c}\mathrm{INR}_n\cdot\left\{(\mathbf{I}_K\otimes(\mathbf{P}\odot\mathbf{D}(\theta_n)))^H(\mathbf{I}_K\otimes(\mathbf{P}\odot\mathbf{D}(\theta_n)))\right\}$; and the superscript r denotes the iteration number of fractional programming for addressing Eq (17). The positive parameter $\lambda^{(r)}$ denotes the output SINR of the rth iteration. Let

$$\begin{aligned}&\mathbf{T}^{(r)}=\left(\mathbf{U}(\theta_t)\text{-}\lambda^{(r)}\left[\boldsymbol{\Sigma}(\theta_n)+\frac{N_r}{M}\mathbf{I}_{MK}\right]\right),\\&\mathbf{W}^{(r)}=\mathbf{T}^{(r)}+\eta\mathbf{I}_{MK}.\end{aligned}\tag{19}$$

where η is a non-negative constant to ensure $\mathbf{W}^{(r)}\succ 0$.

Hence, Eq (18) can be recast as

$$\begin{aligned}&\max_{\boldsymbol{x}}\ \boldsymbol{x}^H\mathbf{W}^{(r)}\boldsymbol{x}\\&s.t.\ \arg x(i)\in[\gamma_i-\alpha,\gamma_i+\alpha],\\&\quad |x(i)|=1\quad i=1,...,MK.\end{aligned}\tag{20}$$

In [26], a generalized power-like iteration method (GPLIM) is adopted to address the non-convex problem in Eq (20). q is used the internal iteration number of the GPLIM. By ignoring the SC of Eq (20), an unimodular vector $\boldsymbol{x}^{(q+1)}$ can obtained by maximizing the objective of the problem in Eq (20), i.e.,

$$\boldsymbol{x}^{(q+1)}=e^{j\arg(\mathbf{W}^{(r)}\boldsymbol{x}^{(q)})}.\tag{21}$$

Further, the phases of the obtained vector $\boldsymbol{x}^{(q+1)}$ should be optimized according to the SC. In particular, denote $\boldsymbol{\phi}=\arg(\mathbf{W}^{(r)}\boldsymbol{x}^{(q)})=[\phi_1,...,\phi_k,....,\phi_{MK}]^T$ and let the phase φ_k of $\hat{\boldsymbol{x}}^{(q+1)}(k)$ satisfy the following equation.

$$\varphi_k=\begin{cases}\phi_k,(\phi_k\pm 2m\pi)\in[\gamma_k-\alpha,\gamma_k+\alpha],m=0,1;\\ \gamma_k-\alpha,\cos(\phi_k-\gamma_k+\alpha)\geq\cos(\phi_k-\gamma_k-\alpha);\\ \gamma_k+\alpha,\cos(\phi_k-\gamma_k+\alpha)<\cos(\phi_k-\gamma_k-\alpha).\end{cases}\tag{22}$$

Finally, the obtained transmit waveform that satisfies the CMC and SC of Eq (20) via the $(q+1)$ th GPLIM is given by

$$\boldsymbol{x}^{(q+1)}(k)=e^{j\varphi_k},\ k=1,...,MK.\tag{23}$$

Suppose a prescribed threshold is κ. Let $\delta^{(q+1)}$ denote the objective function value of the problem given in Eq (20) after the $(q+1)$ th iteration, that is, $\delta^{(q+1)} = \boldsymbol{x}^H \mathbf{W}^{(r)} \boldsymbol{x}\big|_{\boldsymbol{x}=\boldsymbol{x}^{(q+1)}}$; thus, if $\left|\delta^{(q+1)} - \delta^{(q)}\right| < \kappa$, the GPLIM is complete, and the optimal solution of Eq (20) can be obtained. The GPLIM algorithm is summarized as follows.

Algorithm 1: GPLIM for solving Eq (20).

Input: $\mathrm{w}^{(r)}, \varepsilon, \gamma_k, k=1,...,MK$ and a suitable $\boldsymbol{x}^{(r)}$ within the feasible sets of Eq (20)
Output: A suboptimal solution $\bar{\boldsymbol{x}}^{(r)}$ for Eq (20)
1: Set $q=0$ and initialize $\boldsymbol{x}^{(q)} = \boldsymbol{x}^{(r)}$;
2: Compute $\delta^{(q)} = \boldsymbol{x}^H \mathbf{W}^{(r)} \boldsymbol{x}\big|_{\boldsymbol{x}=\boldsymbol{x}^{(q)}}$, $\hat{\boldsymbol{x}}^{(q+1)} = e^{j\arg(\mathbf{W}^{(r)}\boldsymbol{x}^{(q)})}$ and $\boldsymbol{\phi} = \arg(\mathbf{W}^{(r)}\boldsymbol{x}^{(q)})$;
3: Optimize the phases of $\hat{\boldsymbol{x}}^{(q+1)}$ via Eqs (22) and (23) and obtain $\boldsymbol{x}^{(q+1)}(k) = e^{j\varphi_k}, k=1,...,MK$;
4: Calculate $\delta^{(q+1)} = \boldsymbol{x}^H \mathbf{W}^{(r)} \boldsymbol{x}\big|_{\boldsymbol{x}=\boldsymbol{x}^{(q+1)}}$;
5: $q = q+1$, repeat step 2 to step 4 until $\left|\delta^{(q+1)} - \delta^{(q)}\right| < \kappa$;
6: Output $\bar{\boldsymbol{x}}^{(r)} = \boldsymbol{x}^{(q+1)}$.

4.3. Joint Optimization of $\boldsymbol{x}$ *and* $\mathbf{P}$

In this section, the overall joint design of the transmit waveform and array structure for the MIMO radar under interference and noise conditions is summarized in Algorithm 2.

Algorithm 2: Joint optimization algorithm for solving Eq (15).

Input: $\theta_t, \mathrm{SNR}, \mathrm{INR}_n, \theta_n, n=1,...,N_c$, and $\boldsymbol{x}_0, \kappa, \eta$
Output: An optimal solution $(\boldsymbol{x}^*, \mathbf{P}^*)$ to Eq (15)
1: Set $l=0$, initialize $\boldsymbol{x}^{(l)} = \boldsymbol{x}_0$ and compute α, γ_i, $i=1,...,MK$;
2: Optimize P_t、P_r through combinatorial search by maximizing Eq (16) and obtain P_r^*, P_t^*;
3: Use r as the internal iteration number of step 3 and initialize $r=0$;
  3.1: Compute $SNR^{(r)}$, $\lambda^{(r)}$, and $\mathbf{T}^{(r)}$, and update normalized parameters $\mathbf{W}^{(r)}$ with proper η;
  3.2: Exploit **Algorithm 1** to optimize $\boldsymbol{x}^{(r)}$ with Eq (20);
  3.3: $r = r+1$, repeat step 3.1 and step 3.2 until $\left|\lambda^{(r+1)} - \lambda^{(r)}\right| \le \kappa$ for a given κ and proceed to step 4;
4: $l = l+1$, repeat step 2 and step 3 until $\left|\mathrm{SINR}^{(l+1)} - \mathrm{SINR}^{(l)}\right| \le \kappa$, output $\boldsymbol{x}^* = \boldsymbol{x}^{(r)}$ and $\mathbf{P}^* = P_r^* P_t^{*T}$.

The inspection of Algorithm 2 reveals that Algorithm 2 is combined with the sequential optimization, fractional programming, and the GPLIM. Because the sequential optimization and fractional programming algorithms are all convergent [26,20], only the convergence of the GPLIM is considered in this case. Note that at the beginning of Algorithm 2, the initial emission waveform is $\boldsymbol{x}_0$, so that the input $\boldsymbol{x}^{(r)}$ of Algorithm 1 is always within the feasible sets of Eq (20). Denote $\beta^{(q)} = \mathbf{W}^{(r)}\boldsymbol{x}^{(q)}$, according to the phase optimization rule in Eq (22), then

$$\cos(\arg(\boldsymbol{x}^{(q+1)}(k)) - \arg(\beta^{(q)}(k))) \ge \cos(\arg(\boldsymbol{x}^{(q)}(k)) - \arg(\beta^{(q)}(k))), k=1,...,MK. \tag{24}$$

As $\boldsymbol{x}^{(q+1)}$ and $\boldsymbol{x}^{(q)}$ are both unimodular, there is

$$\mathrm{Re}\left\{(\boldsymbol{x}^{(q+1)}(k))^* \beta^{(q)}(k)\right\} \ge \mathrm{Re}\left\{(\boldsymbol{x}^{(q)}(k))^* \beta^{(q)}(k)\right\}, \quad k=1,...,MK. \tag{25}$$

With the definition of Eq (19), $\mathbf{W}^{(r)}$ is a positive Hermitian matrix, that is, $\mathbf{W}^{(r)} \succ 0$, therefore,

$$\mathrm{Re}\left\{(\boldsymbol{x}^{(q+1)})^H \mathbf{W}^{(r)} \boldsymbol{x}^{(q)}\right\} \geq \mathrm{Re}\left\{(\boldsymbol{x}^{(q)})^H \mathbf{W}^{(r)} \boldsymbol{x}^{(q)}\right\} = (\boldsymbol{x}^{(q)})^H \mathbf{W}^{(r)} \boldsymbol{x}^{(q)}. \tag{26}$$

If $\boldsymbol{x}^{(q+1)} \neq \boldsymbol{x}^{(q)}$, we have

$$(\boldsymbol{x}^{(q+1)} - \boldsymbol{x}^{(q)})^H \mathbf{W}^{(r)} (\boldsymbol{x}^{(q+1)} - \boldsymbol{x}^{(q)}) > 0 \tag{27}$$

which implies that

$$(\boldsymbol{x}^{(q+1)})^H \mathbf{W}^{(r)} \boldsymbol{x}^{(q+1)} > 2\mathrm{Re}\left\{(\boldsymbol{x}^{(q+1)})^H \mathbf{W}^{(r)} \boldsymbol{x}^{(q)}\right\} - (\boldsymbol{x}^{(q)})^H \mathbf{W}^{(r)} \boldsymbol{x}^{(q)} \geq (\boldsymbol{x}^{(q)})^H \mathbf{W}^{(r)} \boldsymbol{x}^{(q)}. \tag{28}$$

The inequality chain in Eq (28) proves that Algorithm 1 is monotonously non-decreasing. Further, objective $\boldsymbol{x}^H \mathbf{W}^{(r)} \boldsymbol{x}$ is evidently upper bounded by the maximum eigenvalue of $\mathbf{W}^{(r)}$. Thus, Algorithm 1 is convergent, and as a result, Algorithm 2 is also convergent.

5. Numerical results

In this section, we evaluate the performance of the developed algorithm for joint design emission waveform and array structure of the MIMO radar system with SINR maximization criteria, considering interferences and noise. Unless otherwise stated, we assume that the number of antennas in full-array is $M = 10$, and the numbers of transmit and receive antennas is $N_t = 4$ and $N_r = 8$, respectively. The code length is $K = 36$, and the total transmit energy is $E = M \cdot K$. Without loss of generality, we choose the orthogonal linear frequency modulation (LFM) as the reference waveform, which can be expressed as

$$\mathbf{S}_0(m,k) = \exp\left\{\frac{j2\pi m[(k-1)+(k-1)^2]}{K}\right\} \tag{29}$$

where $m = 1,...,M$ and $k = 1,...,K$. The reference waveform vector $\boldsymbol{x}_0$ can be obtained by stacking the column of $\mathbf{S}_0$. There is only one spatial target, and reflecting energy of target is $|\alpha_t|^2 = 20dB$ from direction $\theta_t = 20°$. The number of the spatial interferences is $N_c = 3$, the locating azimuth set is $\{-50°, 0°, 60°\}$, the corresponding reflecting energy is $|\alpha_1|^2 = |\alpha_2|^2 = |\alpha_3|^2 = 30dB$, and the noise energy is $\delta_n^2 = 30dB$.

By keeping the above simulation parameters constant, the number of optimization combinations for $\mathbf{P}$ is $Q = 9450$. The number of the external iteration is $l = 5$, and the number of internal iterations for GPLIM is $r = 10$. The tolerance of the SINR is $\kappa = 10^{-2}$. The simulation is performed in MATLAB 2018b version, running on a standard PC (with a 2.5GHz Core i7 CPU and 32GB RAM).

5.1. Optimization of waveform $\boldsymbol{x}$ with fixed transmit array vector P_t and receive array vector P_r

In this subsection, we assess the performance of Algorithm 1 in a fixed receive and transmit array structure. Assume that the vectors of transmit and receive array are P_t=[1 0 1 0 1 0 0 0 0 1]^T and P_r=[1 1 1 0 1 1 0 1 1 1]^T, which is just one of 9450 combinations. During alternating optimization, the array vectors P_t and P_r that match with the fixed waveform are selected from all the combinations,

thus maximizing the output SINR. Here, the similarity parameter takes $\varepsilon = 1$. The pulse compression curves of the optimized waveform and reference waveform are shown in Figure 2, which indicates that the pulse compression performance of the optimized waveform is close to the reference waveform under similar constraints; however, the sidelobe is slightly higher.

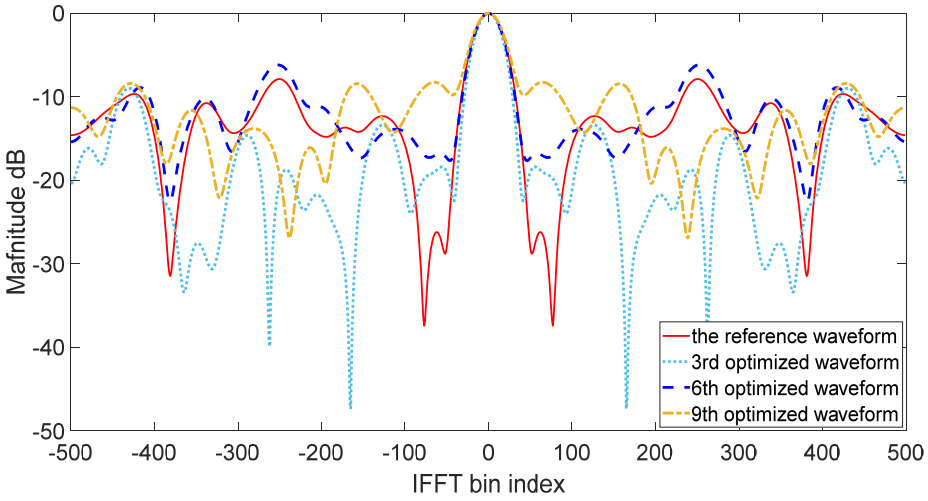

Figure 2. Pulse compression comparison of waveforms.

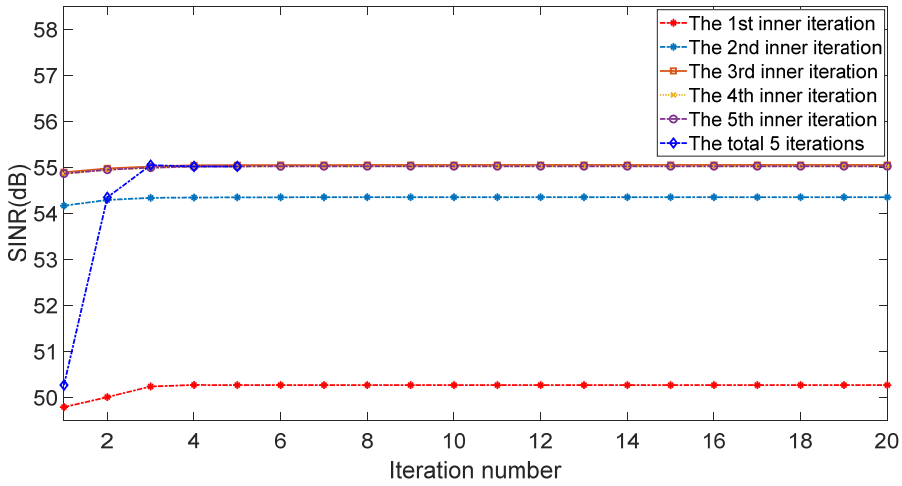

Figure 3. SINR versus iteration number.

Figure 3 illustrates the output SINR versus the inner and outer iteration numbers. The first five curves represent the results of the five executions of Algorithm 1, which is the inner iteration, and each curve consists of 10 internal iteration SINR data. The 6th curve represents the outer iteration, and the SINR converges after five iterations. It can be noted that the objective function of Algorithm 1 based on the GPLIM gradually increases, and the SINR converges to 55.0289 dB after three times for both inner and outer iterations.

After the waveform phase array is transformed into a vector, the phase comparison of optimized sequence and reference sequence is shown in Figure 4. The left two figures are the phase curve of the reference sequence and optimized sequence, and the right is the phase bias between the two phases. The calculations indicate 294 symbols in the optimized waveform sequence have the same

phase as that of the reference sequence. This implies that the similarity constraint works well. As expected, most symbols of the optimized waveform have equal or very similar phase values with the reference waveform.

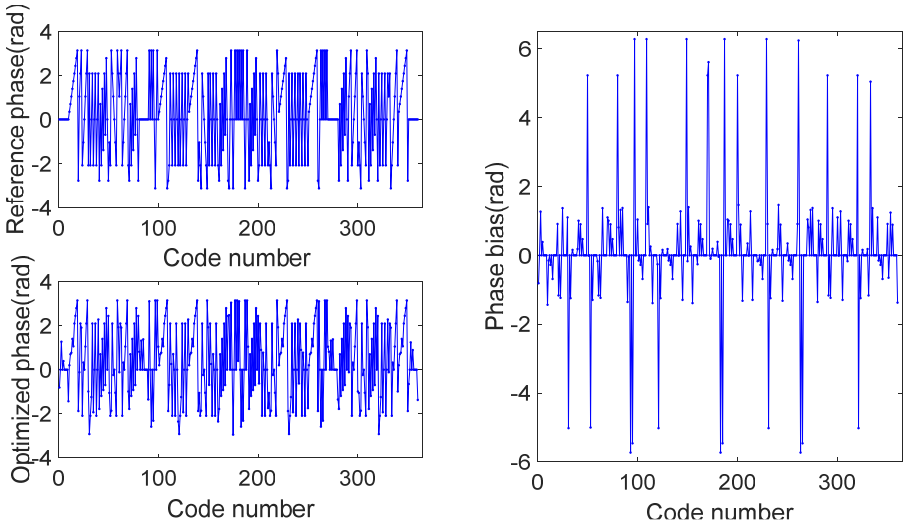

Figure 4. Phase comparison of optimized and reference waveforms.

To demonstrate the convergence of the algorithm, we save the output data of Algorithm 1 as shown in Table 1. As expected, the result indicates that both the inner and outer iteration converge after a relative limited number of executions. The total running time is approximately 2 s.

Table 1. Performance of Algorithm 1.

1st SINR	2nd SINR	3rd SINR	4th SINR	5th SINR
49.7998	54.17242	54.89731	54.86724	54.86901
50.0162	54.29702	54.98079	54.95176	54.95347
50.24706	54.34286	55.02204	54.9961	54.99763
50.27955	54.3499	55.0494	55.02031	55.02203
50.27779	54.35332	55.05274	55.02363	55.02534
50.27667	54.35492	55.05432	55.0252	55.02692
50.27657	54.35572	55.05516	55.02603	55.02774
50.27658	54.35612	55.05562	55.02648	55.0282
50.27658	54.35634	55.05588	55.02675	55.02846
50.27658	54.35646	55.05605	55.02691	55.02862
50.27659	54.35653	55.05615	55.02701	55.02872
50.27659	54.35657	55.05622	55.02707	55.02879
50.27659	54.35659	55.05626	55.02712	55.02883
50.27659	54.35661	55.05629	55.02715	55.02886
50.27659	54.35662	55.05631	55.02717	55.02888
50.27659	54.35662	55.05633	55.02718	55.0289
50.27659	54.35663	55.05634	55.02719	55.02891
50.27659	54.35663	55.05635	55.0272	55.02891
50.27659	54.35663	55.05635	55.0272	55.02892
50.27659	54.35663	55.05636	55.02721	55.02892

5.2. *Joint Optimization of transmit array vector P_t, receive array vector P_r and waveform* $\boldsymbol{x}$

In this subsection, the performance of Algorithm 2 for the joint optimization of the waveform and

array structure is evaluated. Without loss of generality, the numbers of transmit and receive antennas remain $N_t = 4$ and $N_r = 8$, and the code length is still $K = 36$. The similarity parameter is $\varepsilon = 1$, and other simulation parameters remain constant as in part A.

Because the number of P_t and P_r combinations is 9450, it implies that there are many subsequent iterations. To improve the efficiency of optimization, $\mathbf{U}(\theta_t)$ and $\mathbf{\Sigma}(\theta_n)$ under each different group of P_t and P_r are renewed first in Algorithm 2. According to the results in part A, Algorithm 1 converges quickly. The number of outer and inner iterations is set to 5 and 20, respectively. Figure 5 illustrates the optimized array structure, as well as the output SINR versus the inner and outer iteration numbers. Compared with the performance under a fixed pair of P_t and P_r in part A, it can be concluded that with the same prior information of the target, interference, and noise, the joint optimization of array structure and waveforms can obtain higher SINR, which indicates that the joint optimization improves the design freedom and provides better performance. Table 2 shows the detailed output of Algorithm 2 under the optimized array structure; whose convergence is consistent with Algorithm 1.

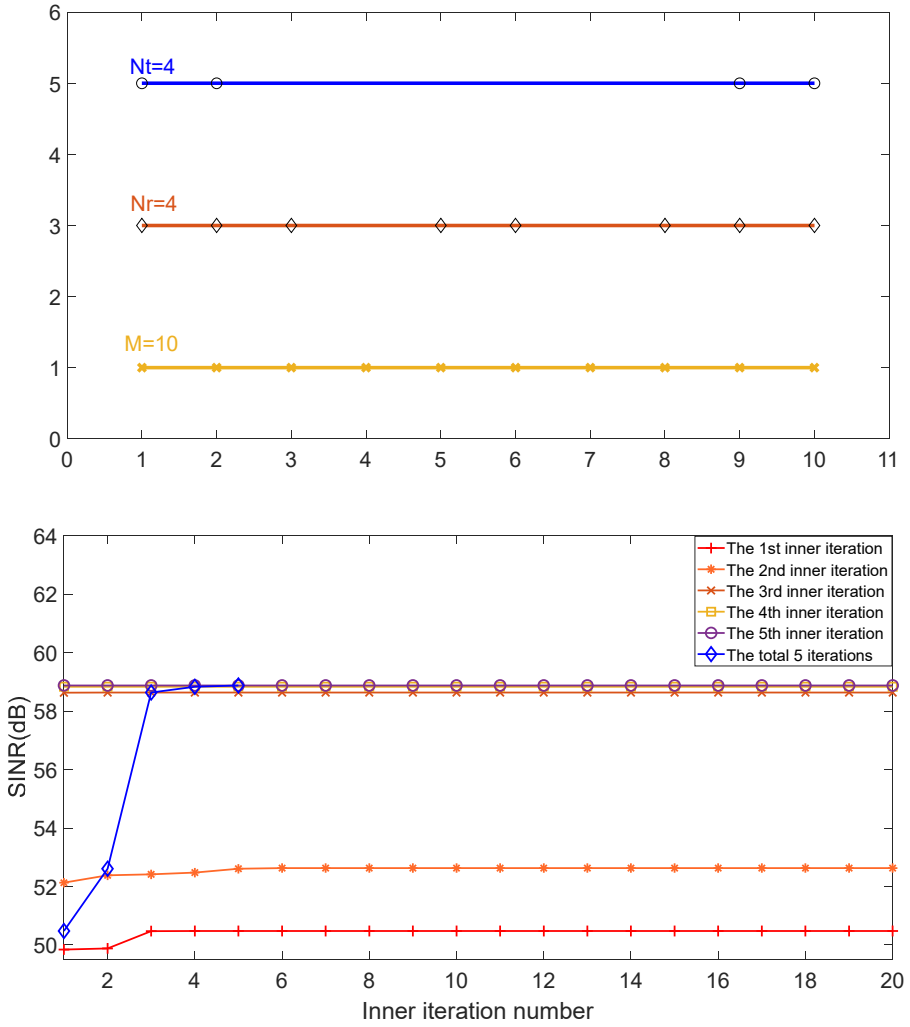

Figure 5. Achieved transmit array vector P_t and receive array vector P_r (above) and SINR versus inner iteration number (below).

Table 2. Performance of Algorithm 2.

1st SINR	2nd SINR	3rd SINR	4th SINR	5th SINR
49.84317643	52.12653358	58.62913039	58.83147542	58.87522621
49.88116039	52.37871535	58.63132757	58.83154403	58.87483263
50.47196236	52.41252103	58.63254229	58.83158156	58.87461766
50.47577922	52.47304948	58.63322803	58.83160245	58.87449832
50.47593723	52.6045335	58.63361998	58.83161425	58.87443103
50.4759836	52.62759847	58.63384642	58.83162102	58.8743925
50.47600588	52.62773403	58.63397857	58.83162495	58.87437012
50.4760181	52.62781443	58.63405642	58.83162727	58.87435694
50.47602497	52.6278625	58.63410269	58.83162865	58.87434909
50.47602885	52.62789135	58.63413041	58.83162948	58.87434435
50.47603104	52.62790869	58.63414714	58.83162998	58.87434147
50.47603228	52.62791913	58.63415729	58.83163029	58.8743397
50.47603297	52.62792542	58.63416349	58.83163048	58.87433861
50.47603337	52.6279292	58.63416729	58.8316306	58.87433793
50.47603359	52.62793148	58.63416963	58.83163068	58.87433751
50.47603371	52.62793285	58.63417107	58.83163072	58.87433724
50.47603378	52.62793368	58.63417197	58.83163075	58.87433707
50.47603382	52.62793418	58.63417252	58.83163077	58.87433697
50.47603384	52.62793448	58.63417286	58.83163078	58.8743369
50.47603385	52.62793466	58.63417308	58.83163079	58.87433686

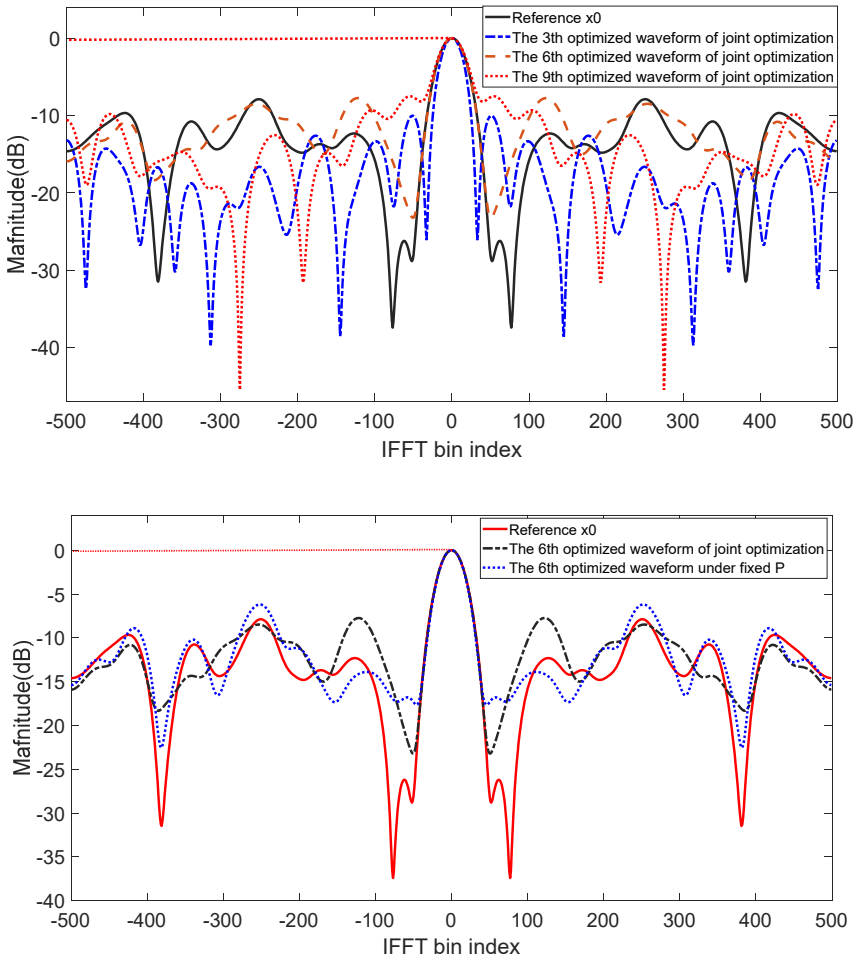

Figure 6. Pulse compression comparison of joint optimization waveforms (above) and pulse compression of three types of waveforms (below).

Similarly, the optimized waveforms are compared with the reference waveform. Figure 6 shows the pulse compression of three different waveforms corresponding to the optimized waveform under the fixed array structure, the optimized waveform under the combined optimization of the transmit waveform and array structure, and the reference waveform, respectively.

By analyzing the pulse compression and SINR figures, Figures 5 and 6, and the corresponding SINR tables, Tables 1 and 2, it is evident that the higher the achieved SINR, the poorer the pulse compression performance. Consequently, it can be concluded that the improved performance of the SINR under the optimized waveform alone or the jointly optimized array structure and waveform is at the price of the waveform pulse compression. Further, it can be observed from Tables 1 and 2 that the former several iterations cause a significant improvement in SINR.

Finally, the similarity constraint of the optimized waveform is examined. The phase and difference between the optimized and reference waveforms are similar to those in Figure 4. In addition, the total number of optimized sequences owning the same phase with the reference vector is 287. Here, Figure 7 adds a subplot to demonstrate the phase error of the optimized waveform relative to the reference waveform.

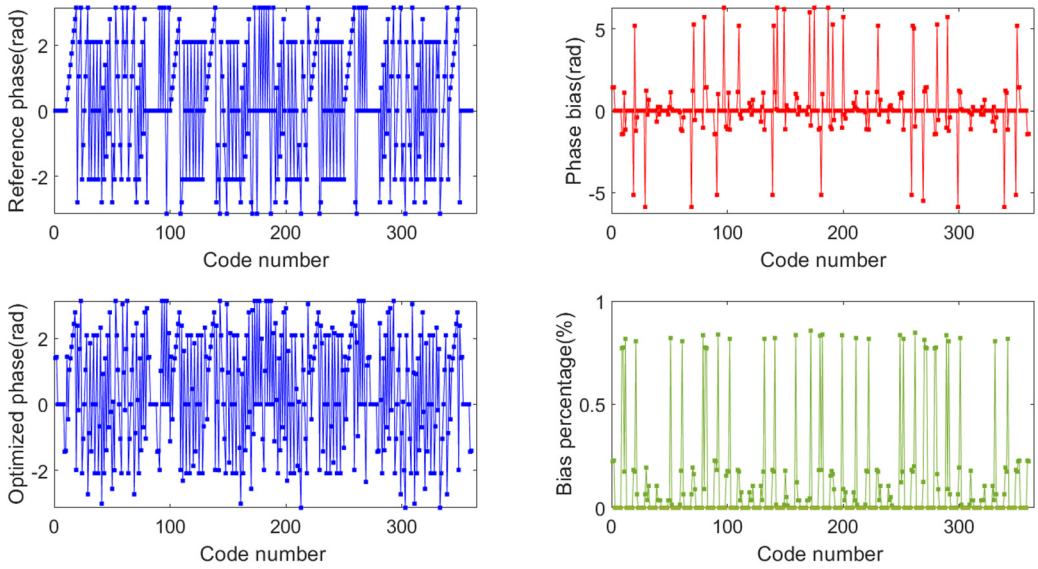

Figure 7. Phase comparison of the optimized waveform by Algorithm 2 and the reference waveform.

6. Conclusions

In this study, the problem of MIMO radar emission waveform and array structure joint design was addressed under the practical constraints of constant modulus and similarity in the presence of signal-dependent interferences and noise. In contrast to the existing methods, which consider waveform optimization or array structure optimization alone, this study takes SINR as the optimization objective and optimizes the design of the transmit waveform and array structure simultaneously, which significantly increases the design freedom. To solve the non-convex problem, a fractional planning and alternating iteration optimization algorithm was deduced. Furthermore, the proposed algorithm was assessed in terms of the performance of both the waveform design under special array structure and waveform design combined with array structure, respectively. In the former scenario, the GPLIM generated waveforms with good pulse compression performance and SINR and converged quickly. In the latter scenario, joint optimization of array structure improved the SINR while keeping the pulse

compression performance almost constant. The simulation results demonstrate the effectiveness of the proposed algorithm. Furthermore, some interesting topics, such as finding a balance between waveform similarity and maximizing SINR, addressing non-independent interference of the signal, and reducing the complexity of joint optimization, will be discussed further in future work.

Acknowledgments

The work was supported by the National Nature Science Foundation of China under Grant 62131020 and 61971434, and in part supported by Hainan Provincial Natural Science Foundation of China under Grant 621QN0872. The authors sincerely thank all reviewers and editors for their careful reading, valuable comments and suggestions on this paper.

Conflict of interest

The authors declare there is no conflict of interest.

References

1. D. J. Rabideau, P. Parker, Ubiquitous MIMO multifunction digital array radar, in *The Thirty-Seventh Asilomar Conference on Signals, Systems & Computers, 2003*, **1** (2003), 1057−1064. https://doi.org/10.1109/ACSSC.2003.1292087
2. E. Fishler, A. Haimovich, R. Blum, D. Chizhik, L. Cimini, R. Valenzuela, MIMO radar: An idea whose time has come, in *Proceedings of the 2004 IEEE Radar Conference*, (2004), 71−78. https://doi.org/10.1109/NRC.2004.1316398
3. H. Fu, H. Fang, S. Cao, M. Lu, Study on the comparison between MIMO and phased array antenna, in *2012 IEEE Symposium on Electrical & Electronics Engineering (EEESYM)*, (2012), 478−482. https://doi.org/10.1109/EEESym.2012.6258697
4. A. Hassanien, S. A. Vorobyov, Phased-MIMO radar: A tradeoff between phased-array and MIMO radars, *IEEE Trans. Signal Process.*, **58** (2010), 3137−3151. https://doi.org/10.1109/TSP.2010.2043976
5. J. Li, P. Stoica, MIMO radar diversity means superiority, in *MIMO Radar Signal Processing*, IEEE, (2009), 1−64. https://doi.org/10.1002/9780470391488.ch1
6. Y. Liu, G. Liao, J. Xu, Z. Yang, Y. Yin, Improving detection performance of passive MIMO radar by exploiting the preamble information of communications signal, *IEEE Syst. J.*, **15** (2021), 4391−4402. https://doi.org/10.1109/JSYST.2020.3009752
7. B. Gao, F. Zhang, G. Sun, S. Pan, High-resolution 3D imaging with a photonics-based broadband MIMO radar, in *2021 International Conference on Microwave and Millimeter Wave Technology (ICMMT)*, (2021), 1−3. https://doi.org/10.1109/ICMMT52847.2021.9618214
8. J. Wang, X. Liang, L. Chen, L. Wang, S. Shi, Joint Wireless Communication and High-Resolution SAR Imaging Using Airborne MIMO Radar System, in *IGARSS 2019 - 2019 IEEE International Geoscience and Remote Sensing Symposium*, (2019), 2511−2514. https://doi.org/10.1109/IGARSS.2019.8897826
9. Y. Zhang, Y. Wang, Z. Tian, G. Leus, G. Zhang, Efficient angle estimation for MIMO systems via redundancy reduction representation, *IEEE Signal Process. Lett.*, **29** (2022), 1052−1056. https://doi.org/10.1109/LSP.2022.3164850

10. C. Chu, Q. Zhang, Y. Chen, MIMO radar waveform joint optimization in spatial-spectral domain for anti-interference, *IEEE Access*, **9** (2021), 160383−160390. https://doi.org/10.1109/ACCESS.2021.3131652
11. N. Chen, P. Wei, L. Gao, H. Zhang, MIMO radar transmit waveform design for joint optimizing beampattern synthesis and spatial autocorrelation performance, in *2021 IEEE 6th International Conference on Computer and Communication Systems (ICCCS)*, (2021), 621−625. https://doi.org/10.1109/ICCCS52626.2021.9449183
12. T. Wei, H. Huang, B. Liao, MIMO radar transmit beampattern synthesis via waveform design for target localization, in *ICASSP 2019 - 2019 IEEE International Conference on Acoustics, Speech and Signal Processing (ICASSP)*, (2019), 4285−4289. https://doi.org/10.1109/ICASSP.2019.8683475
13. H. Chahrour, S. Rajan, R. Dansereau, B. Balaji, Hybrid spread spectrum orthogonal waveforms for MIMO radar, in *2018 IEEE Radar Conference (RadarConf18)*, (2018), 1010−1014, https://doi.org/10.1109/RADAR.2018.8378699
14. L. Xu, H. Liu, Q. Li, S. Zhou, L. Hong, Distributed MIMO radar orthogonal waveforms and mismatched filters design with expanded mainlobe, in *CIE International Conference on Radar (RADAR)*, (2016), 1−5. https://doi.org/10.1109/RADAR.2016.8059149
15. S. Imani, M. M. Nayebi, S. A. Ghorashi, Collocated MIMO radar SINR maximization under ISL and PSL constraints, *IEEE Signal Process. Lett.*, **25** (2018), 422−426. https://doi.org/10.1109/LSP.2018.2796603
16. J. Yang, A. Aubry, A. De Maio, X. Yu, G. Cui, Multi-spectrally constrained transceiver design against signal-dependent interference, *IEEE Trans. Signal Process.*, **70** (2022), 1320−1332. https://doi.org/10.1109/TSP.2022.3144953
17. Y. Chen, Y. Nijsure, C. Yuen, Y. Chew, Z. Ding, S. Boussakta, Adaptive distributed MIMO radar waveform optimization based on mutual information, *IEEE Trans. Aerosp. Electron. Syst.*, **49** (2013), 1374−1385. https://doi.org/10.1109/TAES.2013.6494422
18. A. M. Ahmed, A. Alameer, D. Erni, A. Sezgin, Maximizing information extraction of extended radar targets through MIMO beamforming, *IEEE Geosci. Remote Sens. Lett.*, **16** (2019), 539−543. https://doi.org/10.1109/LGRS.2018.2876714
19. R. Gui, W. Wang, Constant modulus waveforms with restraining spectral interferences for cognitive MIMO radar, in *2017 IEEE Radar Conference (Radar Conf)*, (2017), 0335−0339. https://doi.org/10.1109/RADAR.2017.7944223
20. L. Wang, W. Zhu, Y. Zhang, Q. Liao, J. Tang, Multi-target detection and adaptive waveform design for cognitive MIMO radar, *IEEE Sens. J.*, **18** (2018), 9962−9970. https://doi.org/10.1109/JSEN.2018.2873103
21. Z. Cheng, Y. Liu, Z. He, Y. Li, J. Li, X. Luo, Joint optimization of covariance matrix and antenna position for MIMO radar transmit beampattern matching design, in *2018 IEEE Radar Conference (RadarConf18)*, (2018), 1073−1077. https://doi.org/10.1109/RADAR.2018.8378710
22. A. Bose, S. Khobahi, M. Soltanalian, Efficient waveform covariance matrix design and antenna selection for MIMO radar, *Signal Process.*, **183** (2021). https://doi.org/10.48550/arXiv.2002.06025
23. Z. Cheng, Z. He, B. Liao, M. Fang, MIMO radar waveform design with PAPR and similarity constraints, *IEEE Trans. Signal Process.*, **66** (2018), 968−981. https://doi.org/10.1109/TSP.2017.2780052

24. G. Cui, H. Li, M. Rangaswamy, MIMO radar waveform design with constant modulus and similarity constraints, *IEEE Trans. Signal Process.*, **62** (2014) 343−353. https://doi.org/10.1109/TSP.2013.2288086
25. W. Dinkelbach, On nonlinear fractional programming, *Manage. Sci.*, **13** (1967), 492−498. https://doi.org/10.1287/mnsc.13.7.492
26. H. Wu, Z. Song, Y. Li, Q. Fu, A fast algorithm for designing the transmitted waveform and receive filter of MIMO radar, in *2015 8th International Congress on Image and Signal Processing (CISP)*, (2015), 1363−1367. https://doi.org/10.1109/CISP.2015.7408095

AIMS Press